Laser ablation caused by geometrically constrained illumination and inventive target design

N A Inogamov[1,2], V V Zhakhovsky[2,1] and V A Khokhlov[1]

[1] Landau Institute for Theoretical Physics of the Russian Academy of Scienses, Akademika Semenova 1a, Chernogolovka, Moscow Region 142432, Russia

[2] Dukhov Research Institute of Automatics (VNIIA), Sushchevskaya 22, Moscow 127055, Russia

E-mail: nailinogamov@gmail.com

Abstract. Modern laser technologies use very sophisticated manipulations with (i) a photon cloud forming an irradiation beam and with (ii) disign of a target. E.g. high numerical aperture illumination at very small, diffraction limited conditions is employed for fabrication of the tiny solitary nanoformations on surface of specially prepared thin films deposited onto usually dielectric or semiconductor substrate. In the paper below we list such cases and consider an example with a free standing gold nanofilm modified by tightly focused femtosecond laser pulse.

1. Introduction

Laser technologies in many cases change now more traditional techniques based on thermal, mechanical or chemical treatment. Here we limit ourselves with the list of exotic, state-of-the-art methods of fabrication. All of them use tiny illumination spot (micron size diameter). Thus, contrary to the usually exploited cases with rather large spots ($\sim$ 10–100 μm in diameter), in our situation the lateral effects become determinative. Although, to be honest, there is also the periphery ring around a crater in the large spots. On a bulk targets this periphery is linked to crossing of ablation threshold. Near ablation phenomena on a bulk target need special theoretical consideration [1–6].

Small spot impact is used in a range of different applications. There are LIFT–LIBT laser printing techniques (laser induced forward–backward transfer) [7–12], nanoplasmonic devices (e.g., fabrication of nanoantennas) [13–15], arrays of nanocreations locally amplifying incident weak electromagnetic wave are employed as two-dimensional photon crystals, or for SERS (surface enhanced Raman scattering), or as a booster of photoluminescence [14].

Let us list the five particular small spot cases.

2. Case I: Thin film on substrate

Target geometry is as follows: a thin film, thinner than thickness of a heat affected zone (HAZ) d_{T}, supported by a thick substrate. Weak mechanical coupling between a film and substrate is necessary, weak adhesion (no, e.g., intermediate chromium layer between gold or silver film and substrate). In this case a film easily separates from substrate. The case is sensitive to the value of absorbed energy F_{abs} [10, 11, 16]. Nanocreations (bumps, cupolas, jets, ejection of droplets) appear in a narrow range of energies F_{abs} (few tens of mJ/cm^2) [10, 11, 14, 16]. Below the range

nothing significant is happen. Above the range a simple reach-through hole encircled by a rim remains on a surface of a film covering substrate.

The HAZ d_{T} is thinner than thickness d_{f} of a thin film. For ultrashort pulses the depth d_{T} in a bulk target is achieved during the supersonic stage of the fast conductive expansion of heat initially absorbed in a skin layer. Therefore in the thin case $d_{\mathrm{f}} < d_{\mathrm{T}}$ a whole film is approximately homogeneously heated along its thickness (lateral profile of energy distribution imposed by intensity distribution in a beam remains) prior to the onset of hydrodynamic motion. This is the case when there is symmetry of the vacuum boundary relative to the film-substrate contact along thickness of a film in the sense of homogeneous temperature distribution along thickness. Thus it is of small importance where the frontal (this means light absorbing) surface is. Is radiation comes through vacuum and the frontal boundary is the vacuum boundary of an absorbing film (while the rear-side is a contact between a film and substrate), or is radiation comes through transparent substrate and the contact boundary is at the same time the frontal surface—this is unimportant for subsequent events. The irradiation through substrate corresponds to LIFT, while in LIBT the free surface of a film is illuminated.

Case I is thoroughly studied in our recent papers combining both theoretical understanding and experimental observations [14, 15, 17].

3. Case II: Thick film on substrate

This is the case of a thick film on a substrate: $d_{\mathrm{f}} > d_{\mathrm{T}}$. Let us emphasize that in spite of thickness of a film the presence or absence of the substrate is still definitive. Because we consider thick but not very thick film which may be regarded as a bulk target. In case II the symmetry on temperature distribution prior to motion along thickness between the frontal and the rear-side boundaries of a film is lost.

Irradiation through a transparent substrate is often used to prevent expansion of ablation corona and in this way to amplify the shock sent into a film. This is true for pulses longer than an ultrashort pulse. Shock generated by the ultrashort pulse depends on absorbed energy F_{abs}, for moderate fluences it is less dependent on presence of substrate than in the case of a longer pulse.

The case with irradiation of a thick aluminum film from the substrate side has been considered in [18–20]. Irradiation of a thick silver film from a vacuum side has been studied in experiments [21]. Much more complicated surface structures have been observed in these experiments in comparison with case I [15, 22–24].

The (I) and (II) cases differ. In (I) a film is heated supersonically. After that the positive contact pressure accelerates a motionless matter of a film in the direction out from substrate.

Let us mention that there are two thresholds in case I with weak adhesion [16]. Above the first one, a film overcomes adhesion and flies out from substrate remaining intact. Above the second threshold a film is disrupted in the middle. The vacuum half fly away, while the substrate half remains in contact with substrate with positive pressure at the contact for a long time lasting few acoustic time scales [16]. The contact pressure gradually decays in time. The very late time fate of the substrate half of a film is still not well understood.

If $d_{\mathrm{f}} > d_{\mathrm{T}}$ (case II) then a shock go out from a HAZ at an acoustic time scale $t_{\mathrm{s}} = d_{\mathrm{T}}/c_{\mathrm{s}}$, see [25]. Shock moves matter of a film in the direction opposite to the vacuum side, namely, in the direction to substrate. Shocks refracts on a contact with substrate. One of the questions which arise is: will or not matter of a film separates from the contact in the case of small adhesion? It seems, that as in the case above the second threshold for the situation I, the behavior depends on the internal rupture inside the HAZ- are we below or above the threshold for this rupture called also the ablation threshold. We discuss here the pairs film–substrate with large ratio of the acoustic impedances of a film and substrate (e.g., a gold film on a glass substrate).

4. Case III: Toroidal heating

Another interesting technical innovation for modern manufacturing is connected with illumination through a spiral phase plate creating an optical vortex. The vortex presents a radially polarized laser beam. At the central line-the axis of a vortex-the light waves cancel each other out. Thus a ring type heating of a surface with a dark central area takes place. If we use ultrashort vortex pulse acting on a thin film $d_{\mathrm{f}} < d_{\mathrm{T}}$ then the new nanocreations should appear. They are very different from those which are produced by Gaussian type beam with a maximum of intensity at the optical axis. The diameter of the creations should be small, then, as in Gaussian case I [24], dynamic effects connected with surface tension and, in some extent vapor pressure, plays definitive role.

Circle type heating produces cumulation at the axis [26] even without capillary actions. It is interesting to study in a future work the peculiarities coupled with surface tension.

5. Case IV: Thick free standing film

Free standing means that both surfaces of a film are free—no substrate. Transition between the thin and thick cases has been studied in [27]. In the thin case with fast homogeneous heating the film divided in its middle into two halves above the ablation threshold [28, 29].

The thicker film is inhomogeneously heated. Indeed, HAZ is thinner than d_{f}. When we transit from thin to thick film the ablation threshold increases and the position of the spallation surface slightly above threshold is shifted from the middle plane closer to the frontal (illuminated) boundary. At even thicker film the spallation splits into two different events.

The first one is spallation (or ablation) near a frontal side above threshold F_1. Another one is spallation (not ablation) near the rear-side. It appears above the second threshold $F_2 > F_1$ [18, 20, 27, 30]. This is the today situation concerning the 1D flow of the type (IV). Analysis of the 3D geometry for the targets (IV) needs special investigations. Some understanding follows from the next case V, where the thin, free standing films are considered.

Thin–thick transformation is different for the free standing films (IV, V) and the film-on-substrate targets (I, II).

6. Case V: Thin free standing film

As was said above, the case with 1D (this means a large spot, no lateral phenomena) illumination of a thin film $d_{\mathrm{f}} < d_{\mathrm{T}}$ by ultrashort pulse is well understood [10, 24]. Above ablation threshold the film separates in its middle into two halves flying away. But the 3D case is much more intriguing—for small spots and moderate energies F_{abs} the capillary forces are strong—thus they prevent total separation and prevent the fly away of the halves—surface tension finally returns the halves back. This is a result of a struggle between the inertia and the surface forces.

Inertia and kinetic energy are finite while the surface energy is practically unlimited—it increases and increases proportionally to surface area; we say "practically" because thickness of the stretched film cannot be less than interatomic distance. The area increases with stretching of a film in 3D flow. Thus at first glance surface tension always will win against inertia. But the surface of a stretching half may breaks out. Then some mass will fly away (ablation of this mass).

This situation is similar to the phenomenon with the frozen undersurface bubbles appearing in the rather narrow range around the ablation threshold [1–5]. Small spot, surface tension, crystallization, and 3D geometry increases this range where nucleation of the vapor phase takes place but finally kinetic energy of bubble expansion is not enough to break all cohesive ties of condensed matter.

Below case V for the first time is considered theoretically.

It seems that case V is equivalent to the well studied [10, 24] case I if in case I we will change the underlying substrate to the absolutely unmovable wall. This wall acts as symmetry plane

in the middle of a film with doubled thickness. But this is not totally true: the differences are listed as A, B, and C.

(A) The film–substrate targets considered in (I) [10, 24] have small impedance Z ratio (gold or silver on glass or silicon; the ratio $Z_{\rm s}/Z_{\rm f}$ of substrate to film). This means that the substrate is mechanically soft. Therefore expansion after fast heating of an entire thin film is approximately symmetrical—expansion velocities into the vacuum side $v_{\rm vac}$ with $Z_{\rm vac}/Z_{\rm f} = 0$ is only slightly larger than expansion velocities $v_{\rm s}$ into the substrate side $Z_{\rm s}/Z_{\rm f} \ll 1$. Then the average velocity of a film $v_{\rm sep}(F_{\rm abs})$ after separation is small relative to velocities $v_{\rm s} \approx v_{\rm vac}$.

If velocities $v_{\rm sep}(F_{\rm abs})$ are smaller than it is easier to surface tension to decelerate and stop the flight away. Velocity $v_{\rm sep}(F_{\rm abs})$ increases above the separation threshold $F_{\rm abs}|_{\rm sep} \equiv F_{\rm sep}$ when the value $F_{\rm abs} - F_{\rm sep}$ increases. There is a range of fluences $F_{\rm sep} < F_{\rm abs} < F_{\rm rupt}$ where the separation of a film as whole is possible [16]. Above the threshold $F_{\rm rupt}$ the film breaks out in its middle to two halves [16]. Velocity $v_{\rm sep}(F_{\rm abs} = F_{\rm rupt} - 0)$ slightly below $F_{\rm rupt}$ is few tens of m/s. Velocity of the vacuum side half $v_{\rm vac}(F_{\rm abs})$ quickly increases with $F_{\rm abs}$ above the threshold $F_{\rm rupt}$ achieving soon values ~ 100 m/s [16].

Nanofeatures on the free standing film appears above its rupture threshold $F_{\rm rupt}$ which is close to the rupture threshold for the film–substrate target if the ratio $Z_{\rm s}/Z_{\rm f}$ is small: $Z_{\rm s}/Z_{\rm f} \ll 1$. Velocity of the half of the free standing film $v_{\rm half}(F_{\rm abs})$ is approximately the same function on energy as the function $v_{\rm vac}(F_{\rm abs})$ for the film–substrate if $Z_{\rm s}/Z_{\rm f} \ll 1$.

(B) The film–substrate targets have been simulated in two steps [24]. At the first step we solve the 1D hydrodynamic problem and define the radial velocity profile $v_{\rm sep}(F_{\rm abs})$. After that at the second step we run MD simulation with this velocity profile $v_{\rm sep}(r)v_{\rm sep}[F_{\rm abs}(r)]$ corresponding to the given Gaussian profile $F_{\rm abs}(r)$ of absorbed energy across the irradiated spot.

In the case of the free standing film the first step becomes unnecessary. We homogeneously along thickness of a film heat it. The radial temperature profile is defined by the profile $F_{\rm abs}(r)$: $T(r) \propto F_{\rm abs}(r)$. Thus we start a MD run with the radially heated $T(r)$ and initially motionless film. Results are shown below.

(C) When a film separates from substrate its inner surface is smooth because the contact was smooth. But in the free standing film situation is different. Chaotic nucleation near the middle of a film takes place. Therefore after nucleation during some time a foam like structure exists [2, 3]. Foam connects two halves and during its existence period of time the foam decelerates spatial divergence of the halves. Thus the inner surfaces of the halves are disturbed. But strong capillary forces smooth out the surface perturbations and resists to breaking of the half during its stretching.

7. Scaling approach

Typical smallest sizes of an experimental focal spot are $2R_{\rm L} \approx 0.7$–2 μm. Thickness of a film is $d_{\rm f} = 50$–100 nm. Number of atoms in this volume is $3 \times 10^9\,[L/(1\ \mu{\rm m})]^2\,[d_{\rm f}/(50\ {\rm nm})]$. It is difficult to perform a series of such runs.

Therefore we use scaling to decrease the MD simulation volume. For the problem (I) listed above this approach has been developed in [24]. We postulate that larger in size and smaller in size simulations are approximately equivalent if their capillary number $v_\sigma/v_{\rm half}$ and thermal number $v_\chi/v_{\rm half}$ are the same. Here

$$v_\sigma = 2\sqrt{\sigma/[\rho\,(d_{\rm f}/2)]}, \qquad v_\chi = \chi/R_{\rm L},$$

$v_{\rm half}$ is velocity of a flying half of a film in its central point after rupture of foam, σ is coefficient of surface tension, ρ is density of a film, $d_{\rm f}$ is thickness of a film, $d_{\rm f}/2$ is thickness of a flying half of a film, χ is thermal diffusion coefficient, it defines a rate of cooling of a spot heated by absorption of light, $R_{\rm L}$ is a radius of a focal spot.

Figure 1. Initial stage of expansion of the two half. The gap between the halves is filled with two-phase liquid–vapor mixture. Dynamic interaction between the halves through the stretchable mixture decelerate expansion velocity of the halves. This is the time instant 11 ps, gold film, the film is 10 nm thick before the laser action. After action the maximum temperature is 4 kK. Expansion velocity is 400 m/s. Lateral dimension of this figure is $2R_{\mathrm{L}} = 204$ nm.

Figure 2. The process of rupture of the ties connecting the two halves is almost finished. Instant is 43 ps $\approx 13\,t_{\mathrm{s}}$, $t_{\mathrm{s}} = d_{\mathrm{f}}/c_{\mathrm{s}}$, initial film thickness is $d_{\mathrm{f}} = 10$ nm, $c_{\mathrm{s}} \approx 3$ km/s. Curvature of the shell of the flying half is yet small. Thus deceleration from surface tension is also small. The cross-section along the plane y–z is shown. The tip of the shell passes the axis z, expansion proceeds along the axis z.

Figure 3. Full disintegration of foam. Instant 108 ps. Bubbly liquid from figure 2 corresponding to the instant $t = 11$ ps transforms to mixture of separated liquid droplets and vapor. Now curvature of the shell is enough to appreciably decelerate expansion of the shells. But this is only beginning of deceleration, thickness of a shell remains approximately the same in its tip and its lateral sides.

Rupture of foam takes place after expansion to the distance between the halves of the order of few depths d_{f}. Thickness d_{f} is much smaller than diameter $2R_{\mathrm{L}}$. In 1D ($R_{\mathrm{L}} = \infty$) velocity v_{half} is constant after rupture of foam. But for finite spot the deceleration caused by capillary action slowly decreases velocity $v_{\mathrm{half}}(t)$ at the time scale $R_{\mathrm{L}}/v_{\mathrm{half}}(t = 0)$ and the distances

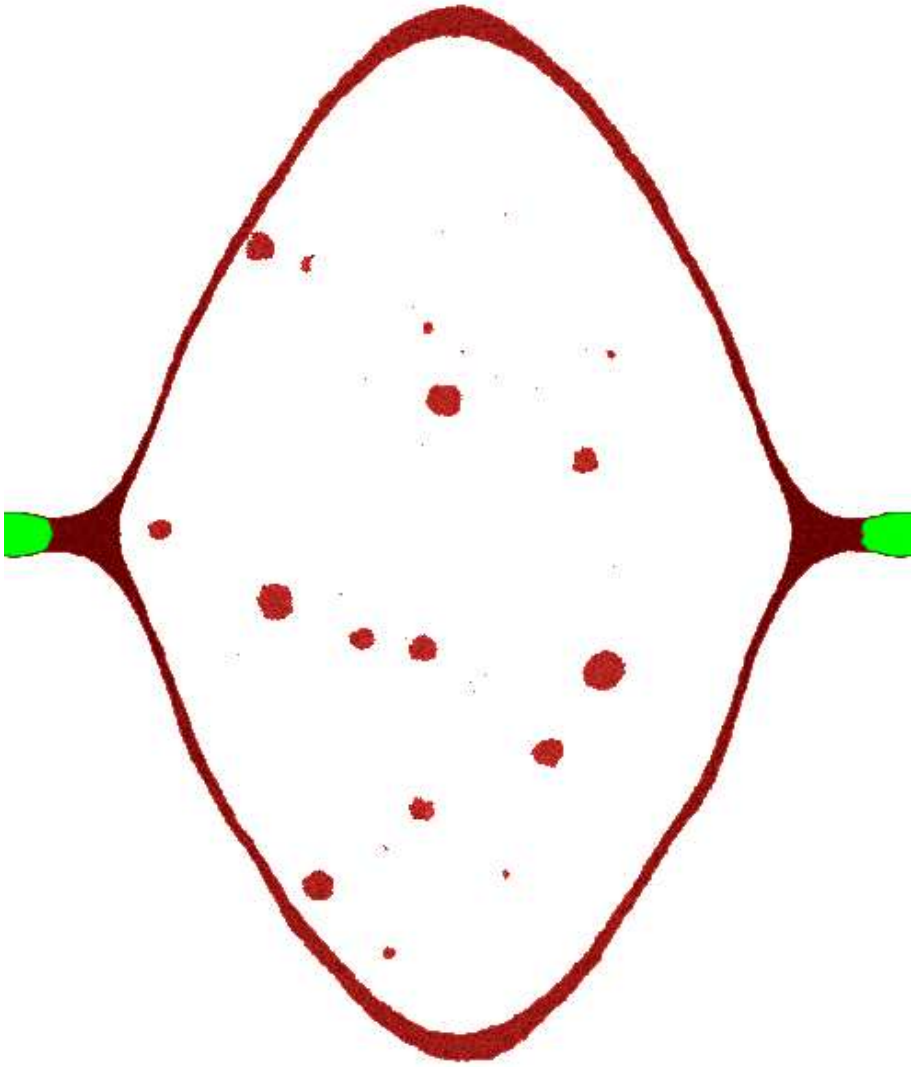

Figure 4. Instant 320 ps. Significant deceleration of expansion of the shell—therefore mass of the shell begins to accumulate in its tip: thickness of the shell is larger in the tip. Due to deceleration the velocity of expansion of the shell decreases. It becomes lower than velocities of some internal droplets. These droplets move faster and impact the shell. Shell survive after these impacts.

between the halves $\sim R_{\rm L}$, here $v_{\rm half}(t=0)$ is velocity of a half after rupture of foam. Time scale $R_{\rm L}/v_{\rm half}(t=0)$ is much longer than the rupture time scale $t_{\rm s}=d_{\rm f}/c_{\rm s}$.

Experimental values are $v_\sigma = 90$ m/s, $v_\chi = 200$ m/s for $\sigma = 1000$ dyne/cm, $\rho = 19.3$ g/cc, $d_{\rm f} = 50$ nm, $\chi = 1$ cm^2/s, $R_{\rm L} = 500$ nm. Velocity $v_{\rm half} \sim 100$ m/s. For velocity $v_{\rm half} = 100$ m/s the non-dimensional numbers are $v_\sigma/v_{\rm half} = 0.9$, $v_\chi/v_{\rm half} = 2$.

In MD simulations we vary $2R_{\rm L} = 140$–204 nm; for our EAM (embedded atom method) interatomic potential of gold (developed in [30]) $\sigma = 540$ dyne/cm [10] slightly above the melting point. Monte-Carlo algorithm used to describe thermal conduction allows us to vary thermal diffusion coefficient. In the MD runs with heating of a free standing film we use thermal conductivity $\kappa = 43$ W/m/K and heat diffusion coefficient $\chi = 0.17$ cm^2/s. The MD $v_\sigma = 210$ m/s for our thickness of a film 10 nm. Velocity $v_{\rm half}(t=0) \approx 400$ m/s. Laser pulse heated the

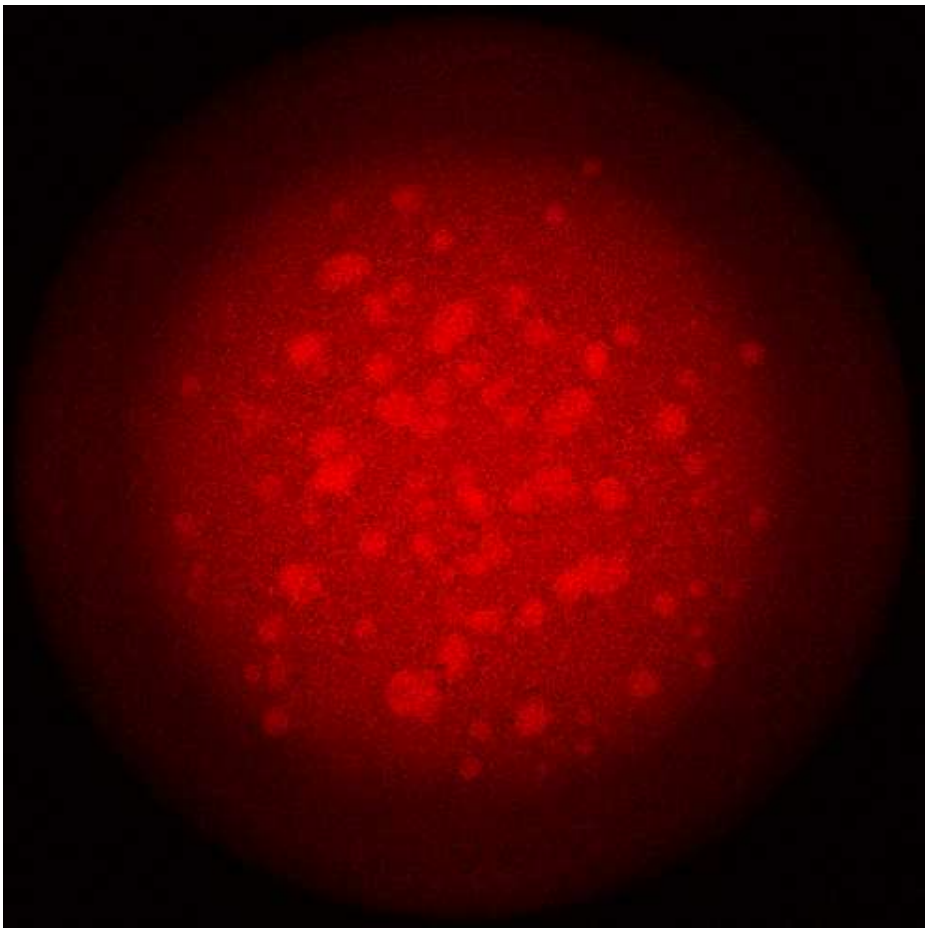

Figure 5. Instant 320 ps. Square has dimensions 204×204 nm^2. Previous figures 1–4 show the lateral view. They are the cross-sections along the plane y–z, where z is direction of expansion. Here the temperature field in the plane x–y is shown. This is the temperatures averaged in every pixel along the axis z. More red colors correspond to higher temperatures. The small bright circles inside the large one are the droplets flying under the shell, see figure 4 for the same instant of time. The droplets lose connection to the shell. Therefore they are more hot than the shell. Because the shell cools down thanks to conductive cooling—the periphery of the shell is kept at the outside temperature. In this run this temperature is 500 K. The large circle is the shell. Not all droplets seen in this picture are shown in figure 4. Because thickness of a cut y–z in figure 4 is rather small relative to the lateral dimension $2R_{\mathrm{L}} = 204$ nm in this run.

MD film up to $T = 4$ kK in the central point of a spot. The heating process was performed by Langevin thermostat during 1 ps.

The MD v_χ = 260–170 m/s. Therefore in the runs presented below the MD thermal number $v_\chi/v_{\mathrm{half}} \approx 0.5$ is less than the experimental one ≈ 2. But it should be mentioned that experimental velocities ~ 100 m/s are poorly known. The capillary numbers are ≈ 1 in experiments and ≈ 0.5 in MD.

8. Results

Figures 1–5 shows development at the initial stage from 11 ps to 320 ps. Acoustic time scale is $t_{\mathrm{s}} = d_{\mathrm{f}}/c_{\mathrm{s}} = 3$ ps for our $d_{\mathrm{f}} = 10$ nm and $c_{\mathrm{s}} \approx 3$ km/s. At the initial stages the fast heating, melting, rarefaction waves interaction, creation of negative pressure inside the film, and

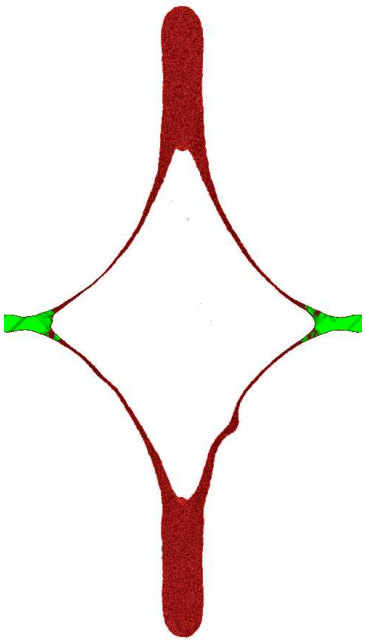

Figure 6. Formation of a jet in the tip of the shell after turning of the shell back from expansion to return at the stage $t \approx 500$ ps. Instant $t = 650$ ps is shown. The shape of the shell changes from the cupola or dome like to the peaked like. At the instant shown, the shell moves back, while the jet continues the motion out. Colors here refer to the central symmetry parameter. Green means that gold is in solid state, while the red color means that in this place molten gold is located. The plane y–z passing through the jet is presented.

nucleation of nanometer size vapor bubbles takes place. These processes finish at acoustic scale t_{s}. We are significantly above threshold for rupture of a film. In this case after nucleation the two-phase liquid–vapor mixture continues to expand.

Volume ratio of liquid to vapor in the mixture decreases as the mixture expand. The ratio passes 50 : 50 stage but percolation through liquid from one half of a film (it gradually takes shape of a shell) to another half-shell survives, and vapor is isolated inside vapor bubbles. The percolation through liquid from shell to shell remains up to rather low volume ratios of liquid. Vapor bubbles transform to the Voronoi type cells. Such cells are limited by liquid thin (relative to dimension of the cell) and approximately plane membranes.

We attribute the stage with foam to the set of the initial stages because its duration is rather short—up to ten t_{s}. After that at beginning of the intermediate stage the membranes in foam break out, later the liquid threads connecting the shells also break down [3]. And foam gradually transforms into the liquid droplets–vapor mixture, see figures 3, 4, and 5.

At the intermediate stage the deceleration significantly reduces expansion velocity of the shells. This reduced velocity becomes lower than velocities of flight of the internal droplets. The droplets overtakes the shell, impact it, and attach to the shell. Integrity of the shell sustains the impacts. Perturbations in the local places of attachments of droplets are rather quickly dumped by surface tension.

There is a cloud of droplets inside the shell, see figures 4 and 5. The cross-sections in figures 4, 6 do not show all of them because volume between the shells around the cross-section plane is rather small relative to the total volume between the shells.

The slowest droplets are flying in the vicinity of the origin—near the point $x = y = z = 0$. Therefore they avoid collision with the shells for a long time. Few of them are still present at

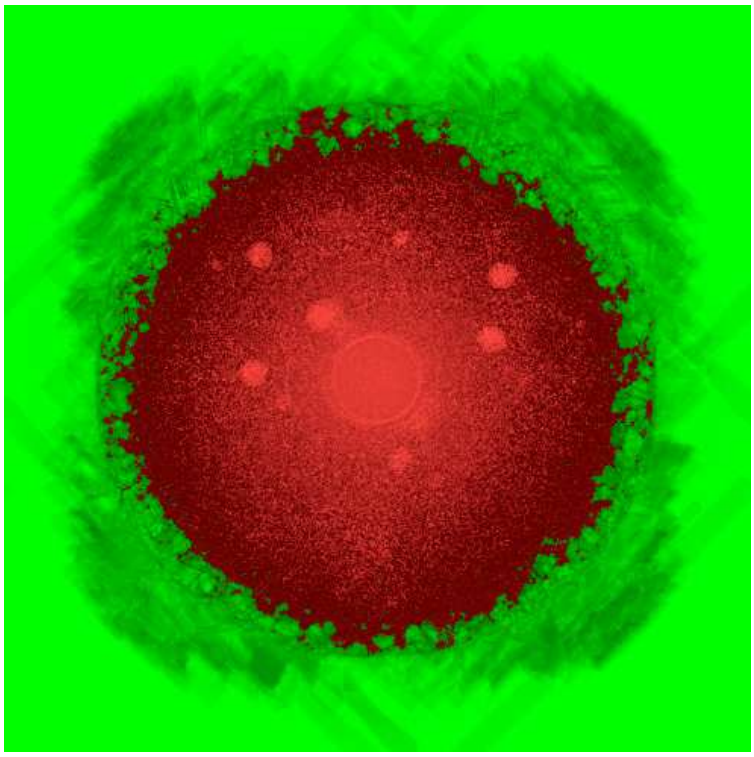

Figure 7. Instant 650 ps is as in the previous figure 6. The central symmetry parameter is shown also (green—solid, red—molten phase). But here the plane x–y is presented. We see the hot droplets (small bright circles), compare with figure 5. The larger bright red circle in the middle relates to the hot gold jet. The jet is absent in figures 5 and 4.

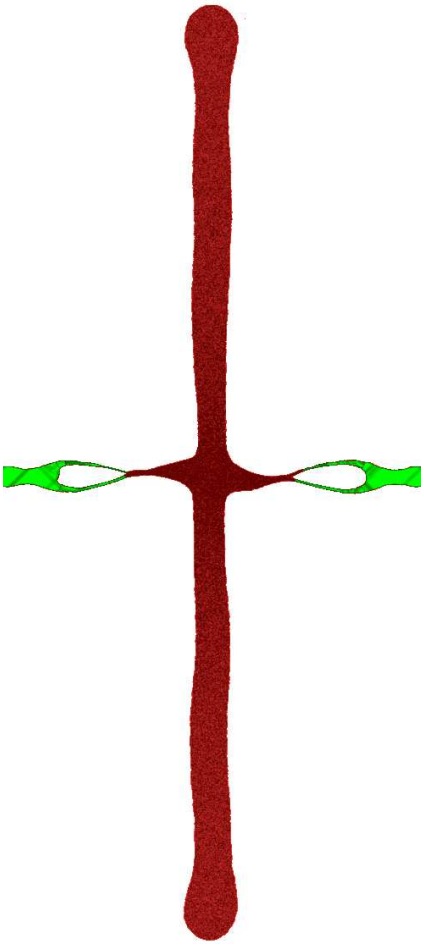

Figure 8. Plane y–z at 1.08 ns.

$t \approx 0.8$ ns. We see that from evolution of the temperature or central symmetry order parameter distributions on a x–y-plane. One of the instant temperature field is presented in figure 5.

Between 400–500 ps the shell stops its expansion. New stage called "stopping and return" begins. The shell starts to move back. Large amount of mass of the shell is accumulated in vicinity of its tip near the instant of stopping, see figure 6. At the stage 500–600 ps the jet begins to grow in the tip of the shell. Curvature of the shell in the plane y–z changes its sign from convex to concave, compare figures 4 and 6.

The forming jet and remaining cloud of hot droplets are well seen in figure 7 corresponding to the instant 650 ps. The jet is the central molten circle. It is larger than the smaller droplets around. At the previous x–y picture in figure 5 this central circle was absent while number of droplets was larger.

The shell continues its return back up to collision with the opposite shell. In the free standing films (V) we have the double shells and the double jets relative to one shell in case I with thin film and substrate [24]. The double jets are not exactly symmetric relative to each other. Collisions of the shells takes place at 900–930 ps. With this collision the final stage begins. The disk is formed thanks to collision.

Figure 8 presents the lateral view on the disk. The disk is formed from matter of the two shells which stick together during their collision. Figures 8 and 9 demonstrates how a solidification

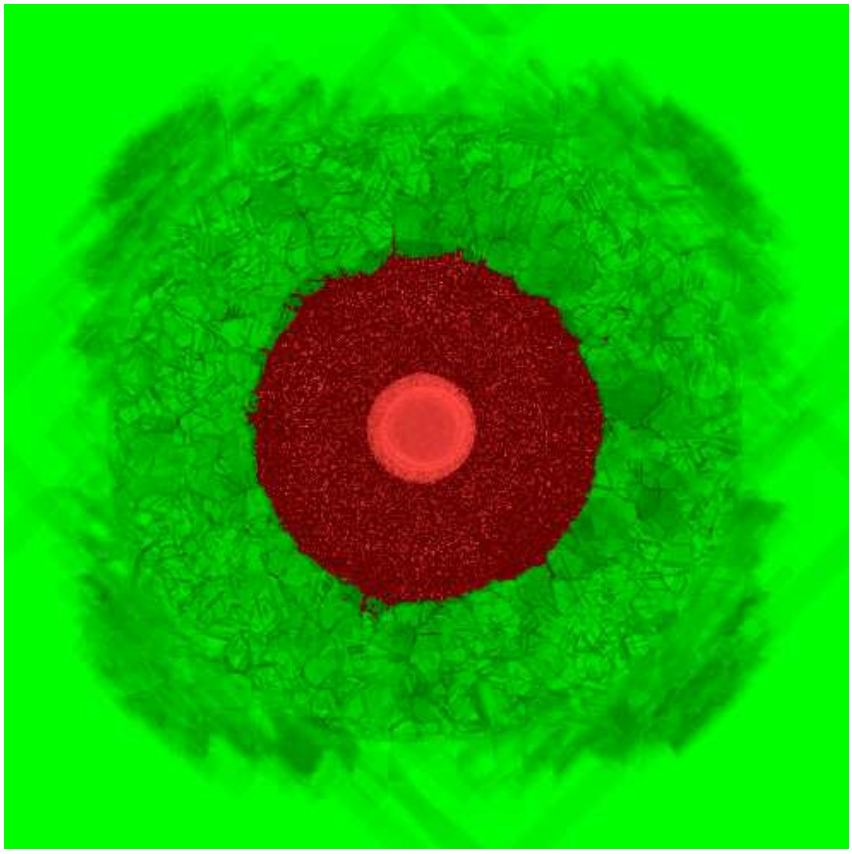

Figure 9. Instant 1.08 ns (as in the previous figure 8), x–y plane. A freezing front begins to transit from the remnants of shell seen in previous figure to the central disk. As it is said in text, the disk is formed by collision of the returning parts of the shells.

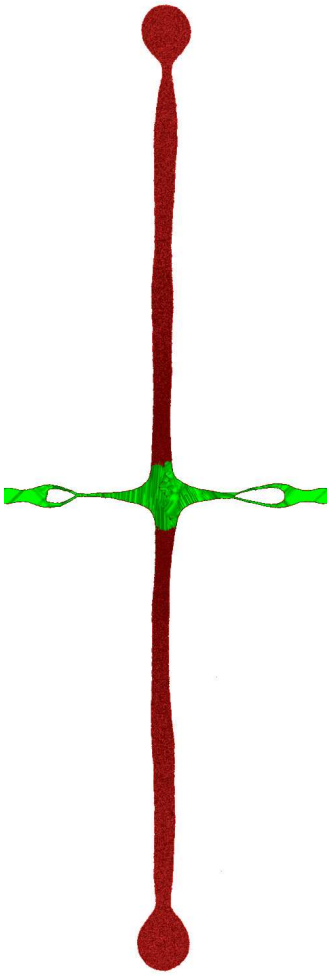

Figure 10. Plane y–z at 2.2 ns. The disk is recrystallized, and solidification now moves along the jet.

zone moving radially in the central direction transits from the solidified remnants of the shells to the disk.

Figures 10 and 11 show that the disk around the jet is totally frozen. During the solidification, disk transforms into unusual crystalline structure. The structure is created from elongated thin plane crystallites (lamellate crystallites) of rather large size. These structures were observed in experiments [31, figure 4]. They puzzled the observers. From MD simulation we see how the family of these crystallites grows. They push one another and squeeze each other in the process of growth. It was more of them per two pi angle around a jet at the initial stage when solidification transits from the shell to the disk in figure 9. But later as solidification proceeds along the disk the larger crystallites close the way to grow for their smaller neighbors. Thus number of them per two pi decreases. Figures 12 and 13 present a final stage. Liquid and solid masses separate at this stage. Liquid fly away leaving or sharp tip or frozen droplet at the tip of the frozen jet. The sharp tips were considered recently in papers [32, 33]. Crystalline structure near the tip may contain 5-fold icosahedral formations [32, 33].

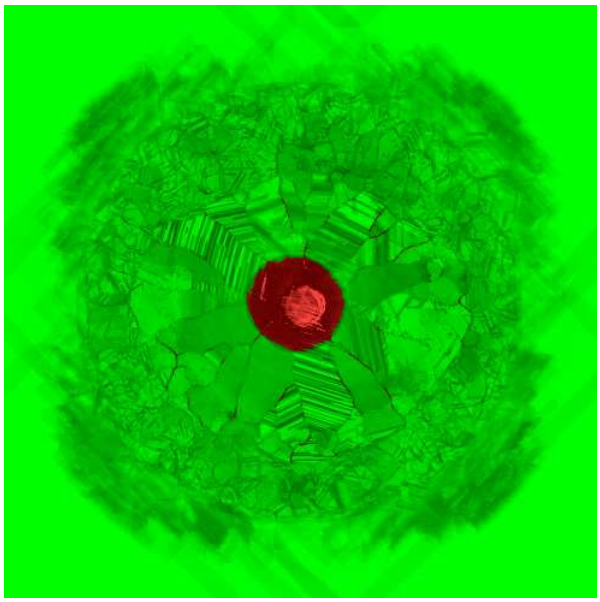

Figure 11. Instant 2.2 ns (as in figure 10), x–y plane.

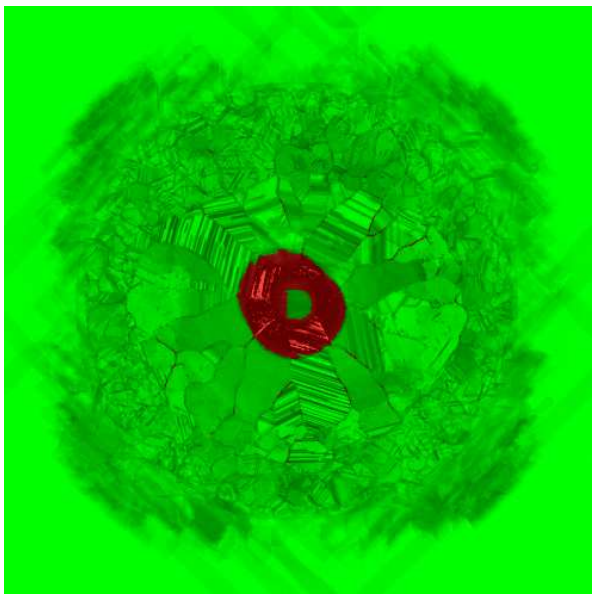

Figure 12. Instant 4.3 ns, x–y plane. The structure of the laminated crystallites is established (compare with figure 11).

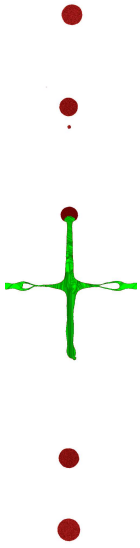

Figure 13. Instant 4.3 ns (as in figure 12), y–z plane. The jets are strongly elongated, the part of them distant from the disk remains liquid. Plateau–Rayleigh instability breaks the jet into liquid droplets.

9. Conclusion

We have considered ultrashort laser action onto thin freestanding film. We show that above ablation threshold the film divides into two halves. Ablation threshold is higher than melting threshold. Thus separation to halves proceeds in liquid state. Capillarity significantly affects dynamics of expansion of the halves. At the early stage of nucleation (stretched liquid nucleates

from random thermal fluctuations) small bubbles in liquid resist to expansion. After that bubbly vapor–liquid mixture transforms to foam like mixture. At this stage surface tension resists to expansion of halves through the membranes in foams. After breaking of membranes the capillary resistance continues through threads remaining from membranes. After breaking of membranes and threads the deceleration of the halves from the internal (bubbles, foam, etc) two-phase structures ceases.

Another decelerator is connected with shells. The halves form the convex shells because of intensity distribution of a beam along irradiated surface. Surface tension acts through curved shells. Of course, this effect is absent in the case of 1D geometry (but the mentioned internal resistance remains, due to foam etc).

Solidification of molten metal described in the paper produces crystallized jets and unusual crystallographic structures around the jet.

Acknowledgments

Authors acknowledge support from the Russian Science Foundation under prolonged grant No. 14-19-01599.

References

[1] Ashitkov S I, Inogamov N A, Zhakhovskii V V, Emirov Y N, Agranat M B, Oleinik I I, Anisimov S I and Fortov V E 2012 *JETP Lett.* **95** 176–81
[2] Inogamov N A *et al* 2014 *J. Phys.: Conf. Ser.* **510** 012041
[3] Inogamov N A *et al* 2014 *J. Phys.: Conf. Ser.* **500** 112070
[4] Wu C, Christensen M S, Savolainen J M, Balling P and Zhigilei L V 2015 *Phys. Rev.* B **91** 035413
[5] Ionin A A, Kudryashov S I, Makarov S V, Levchenko A O, Rudenko A A, Saraeva I N, Zayarny D A, Nathala C R and Husinsky W 2016 *Laser Phys. Lett.* **13** 025603
[6] Li C, Zhang H, Cheng G, Faure N, Jamon D, Colombier J P and Stoian R 2016 *J. Laser Micro/Nanoeng.* **11** 357–65
[7] Korte F, Koch J and Chichkov B N 2004 *Appl. Phys. A* **79** 879
[8] Nakata Y, Miyanaga N and Okada T 2007 *Appl. Surf. Sci.* **253** 6555–7
[9] Ivanov D, Kuznetsov A, Lipp V, Rethfeld B, Chichkov B, Garcia M and Schulz W 2013 *Appl. Phys. A* **111** 675
[10] Inogamov N A, Zhakhovskii V V and Khokhlov V A 2015 *JETP* **120** 15–48
[11] Inogamov N A and Zhakhovsky V V 2016 *J. Phys.: Conf. Ser.* **681** 012001
[12] Inogamov N A, Zhakhovsky V V, Khokhlov V A, Kuchmizhak A A and Kudryashov S I 2016 *J. Phys.: Conf. Ser.* **774** 012102
[13] Kuchmizhak A, Gurbatov S, Vitrik O *et al* 2016 *Sci. Rep.* **6** 19410
[14] Kuchmizhak A, Vitrik O, Kulchin Y, Storozhenko D, Mayor A, Mirochnik A, Makarov S, Milichko V, Kudryashov S, Zhakhovsky V and Inogamov N 2016 *Nanoscale* **8** 12352–61
[15] Danilov P A, Zayarnii D A, Ionin A A, Kudryashov S I, Rudenko A A, Kuchmizhak A A, Vitrik O B, Kulchin Yu N, Zhakhovsky V V and Inogamov N A 2016 *JETP Lett.* **103** 549–52
[16] Khokhlov V A, Zhakhovsky V V, Khishchenko K V, Inogamov N A and Anisimov S I 2016 *J. Phys.: Conf. Ser.* **774** 012100
[17] Wang X W *et al* 2017 *Phys. Rev. Appl.* **8** 044016
[18] Agranat M B, Anisimov S I, Ashitkov S I, Zhakhovskii V V, Inogamov N A, Komarov P S, Ovchinnikov A V, Fortov V E, Khokhlov V A and Shepelev V V 2010 *JETP Lett.* **91** 471–7
[19] Inogamov N A *et al* 2011 *Contrib. Plasma Phys.* **51** 367–74
[20] Ashitkov S I, Komarov P S, Ovchinnikov A V, Struleva E V and Agranat M B 2016 *JETP Lett.* **103** 544–8
[21] Danilov P A, Zayarny D A, Ionin A A, Kudryashov S I, Nguyen T T H, Rudenko A A, Saraeva I N, Kuchmizhak A A, Vitrik O B and Kulchin Y N 2016 *JETP Lett.* **103** 549–52
[22] Emel'yanov V I, Danilov P A, Zayarnyi D A, Ionin A A, Kudryashov S I, Makarov S V, Rudenko A A, Shikunov D I and Yurovskikh V I 2014 *JETP Lett.* **100** 145–9
[23] Zayarny D A *et al* 2015 *JETP Lett.* **101** 394–7
[24] Inogamov N A, Zhakhovsky V V, Khokhlov V A, Petrov Yu V and Migdal K P 2016 *Nanoscale Res. Lett.* **11** 177
[25] Demaske B J, Zhakhovsky V V, Inogamov N A and Oleynik I I 2013 *Phys. Rev.* B **87** 054109 1–9
[26] Andreev N E *et al* 2015 *Laser Part. Beams* **33** 541–50

[27] Demaske B J, Zhakhovsky V V, Inogamov N A and Oleynik I I 2010 *Phys. Rev.* B **82** 064113
[28] Anisimov S I, Zhakhovskii V V, Inogamov N A, Nishihara K, Oparin A M and Petrov Yu V 2003 *JETP Lett.* **77** 606–10
[29] Upadhyay A K, Inogamov N A, Rethfeld B and Urbassek H M 2008 *Phys. Rev.* B **78** 045437
[30] Zhakhovskii V V, Inogamov N A, Petrov Y V, Ashitkov S I and Nishihara K 2009 *Appl. Surf. Sci.* **255** 9592–6
[31] Danilov P A, Zayarny D A, Ionin A A, Kudryashov S I, Nguyen T T H, Rudenko A A, Saraeva I N, Kuchmizhak A A, Vitrik O B and Kulchin Yu N 2016 *JETP Lett.* **103** 549–52
[32] Wu C and Zhigilei L V 2016 *J. Phys. Chem. C* **120** 4438–47
[33] Anisimov S I, Zhakhovsky V V, Inogamov N A, Murzov S A and Khokhlov V A 2017 *Quantum Electron.* **47** 509–21